Criteria evaluation for the transition of cracking modes in a single-crystal nickel-base superalloy

Christian Busse, D. Gustafsson, Frans Palmert, B. Sjodin, P. Almroth, Johan Moverare, Kjell Simonsson and Daniel Leidermark

Busse, C., Gustafsson, D., Palmert, F., Sjodin, B., Almroth, P., Moverare, J., Simonsson, K., Leidermark, D., (2020), Criteria evaluation for the transition of cracking modes in a single-crystal nickel-base superalloy, *Theoretical and applied fracture mechanics (Print)*, 106, 102453. https://doi.org/10.1016/j.tafmec.2019.102453

Criteria evaluation for the transition of cracking modes in a single-crystal nickel-base superalloy

C. Busse[a,*], D. Gustafsson[c], F. Palmert[b], B. Sjödin[c], P. Almroth[c], J.J. Moverare[b], K. Simonsson[a], D. Leidermark[a]

[a] *Division of Solid Mechanics, Linköping University, SE-58183 Linköping, Sweden*
[b] *Division of Engineering Materials, Linköping University, SE-58183 Linköping, Sweden*
[c] *Siemens Industrial Turbomachinery AB, SE-61283 Finspång, Sweden*

Abstract

Single-crystal nickel-base superalloys frequently experience two distinct fatigue crack growth modes. It has been observed that, under certain conditions, cracks transition from a path perpendicular to the loading direction to a crystallographic slip plane. As crystallographic cracking is associated with an increased fatigue crack growth rate, it is important to be able to predict when this transition occurs. In this work three different criteria for crystallographic cracking based on resolved anisotropic stress intensity factors are evaluated in a three-dimensional finite element context. The criteria were calibrated and evaluated using isothermal fatigue experiments on two different specimen geometries. It is suggested by the results, that a threshold value of a resolved shear stress intensity factor can act as a conservative criterion indicating cracking mode transition. Further, a trend hinting towards a loading frequency dependency could be observed.

Keywords: Single-crystal nickel-base superalloys, Finite element analysis, Fracture mechanics, Resolved stress intensity factor, Crystallographic cracking

*Corresponding author, Tel.: +46 700 89 6003
Email address: christian.busse@liu.se (C. Busse)

1. Introduction

The traditional way in the design process of gas turbines industry has been to assess failure in components made of single-crystal nickel-base superalloys based solely on the crack initiation life. However, with more computational power and advanced tools combined with increased knowledge about the crack growth behaviour in these materials, the failure prediction of such components can now also include the time spent during stable crack growth. This will not only allow for an increased service life but also reduce the environmental footprint due to more optimal designs allowing for higher firing temperatures [1]. Furthermore, the economical profit surrounding the inclusion of crack propagation in the design process is also beneficial.

The rising temperature puts great demand on the exposed materials. This is especially the case for the blades in the first turbine stage which are also exposed to high mechanical loads. To meet these high requirements the blades are generally cast from nickel-base superalloys, which are developed to perform well in this environment with their exceptional high temperature properties. These blades are frequently cast in single-crystal form in order to improve the creep and oxidation properties. As the machines are exposed to more frequent start-ups and shut-downs, due to the role as power grid regulators of intermittent renewable energy sources, thermo-mechanical fatigue conditions generally apply due to the cycling of temperature as well as mechanical loads. A critical location in the blade design is the blade fir tree root, where the temperatures during normal operation rarely exceed 500°C in a stationary gas turbine. As the differences of the material properties associated with the temperature cycling are small, the loading conditions can be approximated as low-cycle fatigue with the constant temperature of 500°C. In this work, focus is thus directed to this area of the blade and associated loading conditions.

The inherent crystallographic structure of single-crystal nickel-base superalloys results in a complex material behaviour, which leads to many challenges in testing, modelling and prediction of the crack initiation and growth be-

haviour [2–8]. It has frequently been observed that two distinct cracking modes are present in these materials; crystallographic cracking on the octahedral {111}-planes and Mode I cracking perpendicular to the loading direction [9–14], *cf.* Fig. 1. It should be noted that Mode I cracking is considered from a macroscopic point of view in this study, where microscopic local crack growth on conjugate slip planes in a zigzag fashion is disregarded. Thus, in this study a transition of cracking modes will be considered to have occurred when reaching stable crystallographic growth that is not overtaken by Mode I crack growth. Palmert *et al.* [15] have shown that for the alloy considered in this study, the highest propensity for crystallographic cracking is at 500°C. Furthermore, previous studies have shown that the crystallographic Fatigue Crack Growth Rate (FCGR) is generally higher compared to Mode I FCGR [16, 17]. Thus, from an industrial point of view it is important to be able to predict when a transition of cracking modes occurs. This is also the main objective of the current work. Hence, a fatigue design approach accounting for the entire chain of the fatigue and fracture history, *i.e.* time spent until crack initiation, Mode I and crystallographic crack growth is beneficial for the industry, as the transition of cracking modes constitutes great risk for failure of the component in ques-

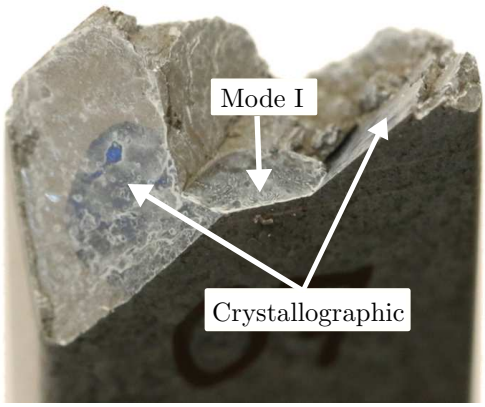

Figure 1: Fracture surface of a surface flawed fatigue crack growth (Kb) specimen showing the two distinct cracking modes.

tion. To the authors knowledge there is currently no model for the prediction of the fatigue life for combined Mode I and crystallographic crack growth in a 3D Finite-Element (FE)-context. Consequently, the fatigue life associated only with Mode I crack growth is generally used, combined with a high safety factor. The time spent during Mode I crack growth is easier and more reliable to predict compared to crystallographic cracking, and is associated with a lower safety factor and therefore giving a less conservative fatigue life prediction. However, in the current literature there is no consensus about a criterion describing the transition between cracking modes. Telesman and Ghosn [9] argued that the onset for crystallographic crack growth is related to the loading frequency and temperature, where a lower frequency, combined with high temperatures, promotes non-crystallographic Mode I crack growth that is driven by an environmentally controlled damage process. If the embrittlement at the crack tip occurs at a higher rate than the crack growth rate through a crystallographic damage mechanism, then the crack growth will occur in a Mode I fashion. If on the other hand there is not sufficient embrittlement, crack growth on the crystallographic plane with the highest Resolved Shear Stress (RSS) will occur. This behaviour is promoted by low temperatures and high loading frequencies. Reed et al. [18] introduced a two-factor criterion for predicting the transition of cracking modes. They claim that i) the ratio of the RSS to the Resolved Normal Stress (RNS) of a slip system on a crystallographic plane expressed in terms of a Resolved Stress Intensity Factor (RSIF) ratio must be at least $\sim$0.45 and i) a sufficient equivalent RSIF incorporating all modes of fracture must be present for crystallographic cracking to occur. Furthermore, much of the research concerning the transition from Mode I to crystallographic cracking states that the maximum RSS on the slip planes is the deciding measure that controls the active slip plane [9, 14, 19], *i.e.* the slip plane on which the crack continues to grow after transition. Often, the Resolved Shear Stress Intensity Factor (RSSIF) is deemed to be the deciding measure controlling the crystallographic crack path [8, 14, 17, 19, 20], and is thus also assumed to play an important role in the transition of cracking modes.

Chen and Sakaguchi [21] recently published a study that investigated the transition behaviour in single-crystal nickel-base superalloy at 450°C according to the slip plane activity computed by a crystal plasticity FE-analysis. They also concluded that shearing (in terms of a damage parameter based on shear strains) plays a major role in the transition of cracking modes.

In this study three different criteria for the transition of cracking modes were evaluated. They were based on isothermal fatigue crack growth experiments conducted at 500°C on two different specimen geometries. The three criteria were; *i*) a threshold value of the RSSIF, *ii*) a crack growth rate criterion based on the work by Reed et al. [18] and *iii*) a crack growth rate criterion inspired by Kagawa and Mukai [12].

Further, the crystallographic orientation plays a vital role in the crack growth behaviour as it influences the material response, and thus the Crack Driving Force (CDF) [12, 14, 19, 22, 23]. Therefore, the crystallographic orientations including the misalignments that were present in the tested specimens were accounted for in this study.

2. Material and Experiments

The material considered in this study is a single-crystal nickel-base superalloy of face-centred cubic structure, similar to the alloy presented by Reed et al. [24]. Its main alloying elements, in order of decreasing wt %, are as follows: Ni-Cr-Ta-Co-Al-W-Mo-Si-Hf-C-Ce.

Two different specimen types were used in the experiments; a surface flawed fatigue crack growth specimen of Kb-type [25], henceforth denoted as Kb specimen, and Disc-Shaped Compact Tension (DCT) specimens with two different nominal thicknesses. Both specimen types were manufactured from cast bars with the casting direction parallel to the nominal [001] crystallographic direction. The geometries and the nominal orientations of the specimens can be seen in Fig. 2. Note that the machined surface flaw in the Kb specimens is centred on the flat surface with the normal [100]. In most of the tested specimens the

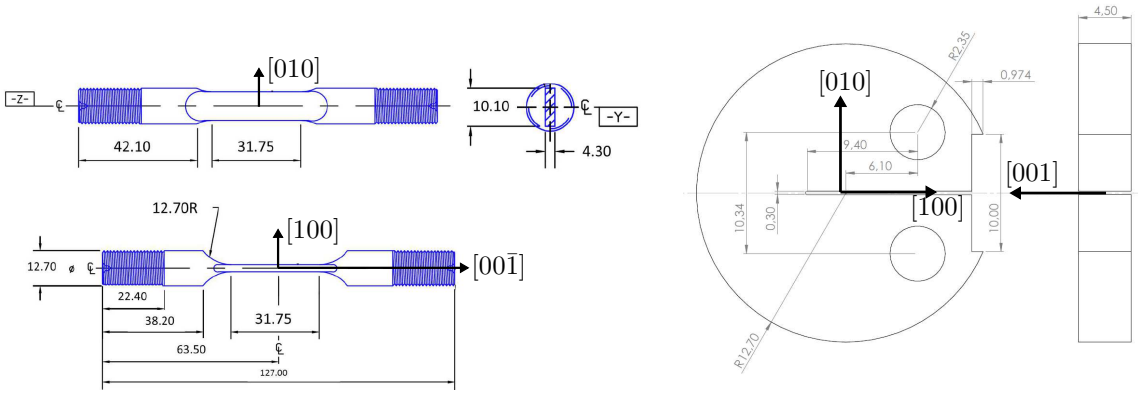

(a) (b)

Figure 2: Technical drawing of (a) the Kb specimen and (b) the DCT specimen with dimensions in mm and the nominal primary and secondary orientations marked. Note that the thickness of the DCT specimen varies for the different specimens as shown in Table 2.

loading direction is of ⟨001⟩-type corresponding to the loading direction typically found in turbine blades, as it entails the direction of lowest stiffness. For some DCT specimens, the loading direction corresponds to a different crystallographic orientation resulting from a rotation of the crystal about the nominal [001] direction, *cf* Fig. 2. The crystallographic orientations of all specimens in terms of sequential rotations about the nominal [010], [100] and [001] directions are shown in Table 1. They were determined by evaluating the visible dendrites representing the projections of the crystallographic lattice vectors on three polished and etched orthogonal surfaces on the specimens. For a detailed description see [19].

Isothermal fatigue crack growth experiments at 500°C were performed according to ASTM E647 [26], where the temperature of 500°C was chosen since it, as previously mentioned, represents the temperature during service at the blade fir tree root, which is a critical location in the blade design. Relevant testing parameters of the experiments are shown in Table 2. Post-experimental treatment by separating the specimen into two pieces made it possible to determine the first occurrence of stable crystallographic growth, and subsequently

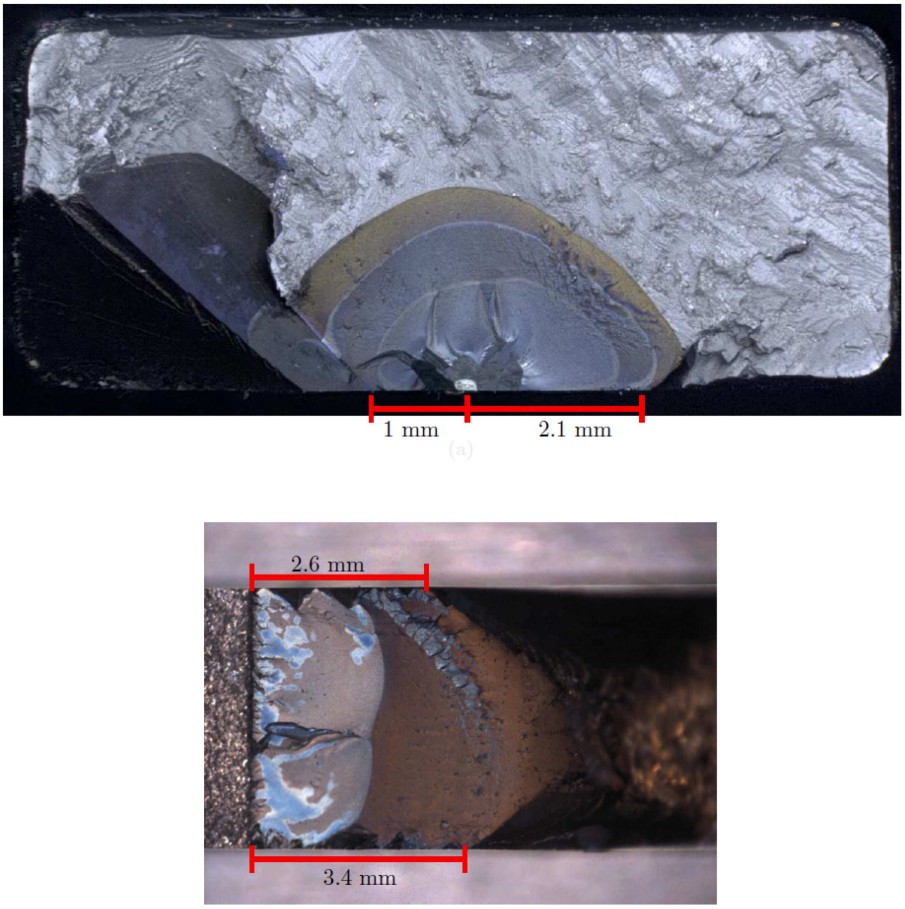

Figure 3: Measurements of the transition crack lengths on the fracture surface of the Kb107 (top) and the DCT07 (bottom) specimens.

the transition crack length was measured. This is exemplified in Fig. 3 where the crack length measurements are shown for the specimens Kb107 and DCT07. The measurements of the first transition along the Mode I crack front correspond to the values shown in Table 2. Further details of the experimental procedure can be found in [19]. Furthermore, the specimens possess anisotropic properties, since they were cast as single-crystals, and the elastic stiffness constants for 500°C can be seen in Table 3.

In [19], a closer look has also been taken at the Mode I fracture surface of

DCT07 (DCT1 in [19]). In the areas where the crack grew orthogonal to the loading direction, it can be seen in a higher magnification scanning electron microscope image, that the γ'-particles have not been sheared and the crack grew in the γ-matrix. The magnification of the image is not high enough to conclude if crack growth occured along two conjugate microscopic slip systems or as a non-crystallographic failure mode. Regardless, as the crack avoided the γ'-particles and grew in the interface, considering the context of this work, which is from an engineering point of view, the cracking mode which is perpendicular to the loading direction is macroscopically regarded as a Mode I crack. Additional fractographic investigations of the DCT specimens can be found in [15].

Table 1: Crystallographic orientation accounting for the misalignment in terms of sequential rotation about the [001], [010] and [100] nominal directions, as defined in Fig. 2.

	Rotation about [°]		
Specimen	[001]	[010]	[100]
DCT07	5.38	-0.16	-4.66
DCT08	19.95	0.14	-6.40
DCT09	46.40	3.24	-2.02
DCT19	2.71	3.64	-3.64
DCT29	1.68	1.62	0.32
DCT30	1.28	1.18	1.38
DCT35	-26.65	2.18	-2.84
DCT36	27.51	0.48	2.06
DCT38	6.19	0.56	-0.72
DCT39	-51.85	-0.52	-0.55
Kb07	-2.82	0.01	1.67
Kb107	-7.65	-4.94	6.29
Kb3-6	-3.40	2.20	0.12

Table 2: Overview of the test conditions in the experiments for all specimens. The testing temperature was 500°C in all experiments.

Specimen	Loading ratio R_σ [-]	Loading frequency f [Hz]	Maximum force [N]	Specimen thickness [mm]	Transition crack length [mm]
DCT07	0.1	0.025	911	4.1	2.6
DCT08	0.1	0.025	871	3.92	2.4
DCT09	0.1	0.025	911	4.1	3.4
DCT19	0.1	0.025	911	4.44	3.1
DCT29	0.1	0.025	1978	8.9	2.63
DCT30	0.1	0.025	1319	8.9	1.76
DCT35	0.1	0.1	697	4.46	2.4
DCT36	0.1	0.1	880	4.46	1.99
DCT38	0.1	0.1	880	4.46	1.98
DCT39	0.1	0.1	880	4.46	2.65
Kb07	0.05	0.5	19857	4.30	0.95
Kb107	0.05	0.5	15858	4.30	1.0
Kb3-6	0.05	0.5	18407	4.30	0.98

Table 3: Elastic stiffness constants, units in GPa.

Temp. (°C)	C_{11}	C_{12}	C_{44}
500	201.9	127.0	112.8

3. Transition of cracking modes

3.1. Crack driving force parameters and crack growth models

In order to evaluate the singular stress field around a crack tip in single-crystal nickel-base superalloy materials for Mode I crack growth the Stress Intensity Factor (SIF) has been proven to be an appropriate measure. To evaluate crystallographic crack growth, anisotropic SIFs resolved onto the slip planes in the slip directions have been shown to be a more suitable entity, *cf.* [9, 19]. The CDF parameters k_I, k_{II} and k_{III} adopted from Busse *et al.* [19] have been used in this study. They are based on the anisotropic SIFs (K_I, K_{II} and K_{III}), which can be evaluated with several techniques. The approach in this work was to use the M-Integral [27] incorporating anisotropic material properties and accounting for the crystallographic orientations including the material misalignments. The anisotropic SIFs have been used to reconstruct the singular stress field near the crack tip based on the equations developed by Hoenig [28] for generally anisotropic materials. The corresponding stress tensor was then multiplied by $\sqrt{2\pi r}$ and resolved (projected) on the 12 slip systems to evaluate the RSIFs. For each slip system, the RSIFs; k_I (corresponding to the normal to the crystallographic plane), k_{II} (primary slip direction) and k_{III} (secondary slip direction) were determined, cf. Fig. 4 for a schematic representation of these on a crystallographic plane. Further information can be found in [19]. These RSIFs associated with the three modes of loading resolved on the crystallographic planes in the slip directions and are consequently defined accordingly:

- The resolved normal stress intensity factor:

$$k_{RNS} = k_I \tag{1}$$

- The resolved shear stress intensity factor:

$$k_{RSS} = \sqrt{k_{II}^2 + k_{III}^2} \tag{2}$$

- The equivalent resolved stress intensity factor:

$$k_{EQ} = \sqrt{k_{RNS}^2 + k_{RSS}^2} = \sqrt{k_I^2 + k_{II}^2 + k_{III}^2} \tag{3}$$

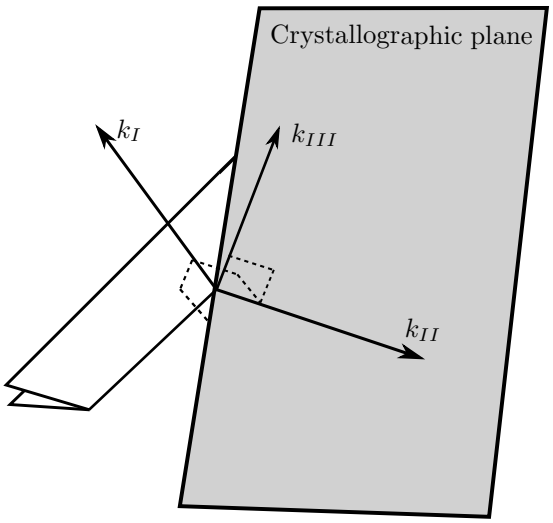

Figure 4: Illustration of the directions associated with the RSIFs on a crystallographic plane for one slip system, where k_{II} corresponds to the primary slip direction, k_{III} to the secondary slip direction and k_I to the normal of the crystallographic plane.

The above CDFs were used in the modelling procedure of the crystallographic crack growth rate. The FCGRs for both cracking modes, Mode I and crystallographic growth, were evaluated in Busse *et al.* [17], where the following crack growth models were quantified;

- For crystallographic crack growth, with the crystallographic crack length L:

$$\frac{dL}{dN} = C_c(\Delta k_{RSS})^{n_c}, \tag{4}$$

where $n_c = 4.75$ and $C_c = 4.87 \cdot 10^{-8}$ for k_{RSS} in MPa$\sqrt{m}$ and dL/dN in mm/cycle.

- For Mode I crack growth:

$$\frac{da}{dN} = C_I(\Delta K_I)^{n_I}, \tag{5}$$

where $n_I = 2.68$ and $C_I = 3.91 \cdot 10^{-8}$ for K_I in MPa$\sqrt{m}$ and da/dN in mm/cycle.

3.2. Evaluated transition criteria

Three criteria to predict the transition of cracking modes were evaluated in this work. It should be noted, that only the transition from Mode I to crystallographic cracking is considered and not vice versa, as the latter did not happen in the evaluated experiments. Further, only the first stable transition to a crystallographic plane along the crack front is considered. The criteria were applied for the crack front shape present at the transition crack length.

1. k_{RSS} **threshold criterion**

   The idea behind a threshold RSSIF criterion is that crystallographic cracking is associated with the shearing of the γ'-particles and thus also with k_{RSS}. Further, damage on the crystallographic planes is accumulated by dislocation movement on these planes, which is the prevailing slip mode in face-centred-cubic materials [14], and the damage is thus directly coupled to the RSSes.

2. **FCGR criterion**

   This criterion, inspired by the work of Kagawa and Mukai [12], is based on the assumption that a crack always chooses the path of least resistance, *i.e.* highest energetic efficiency, meaning that transition will occur once the FCGR of crystallographic cracking exceeds the Mode I growth rate. In this work, the FCGRs given by the crack growth models presented in [17], *cf.* Eqs 4 and 5, were evaluated at the transition crack length observed in the experiments and compared to each other by defining the ratio of the crystallographic to the Mode I FCGR:

   $$X = \frac{C_c(\Delta k_{RSS})^{n_c}}{C_I(\Delta K_I)^{n_I}} \tag{6}$$

3. **Two-factor criterion**

   This model is based on the two-factor criterion as presented in the work

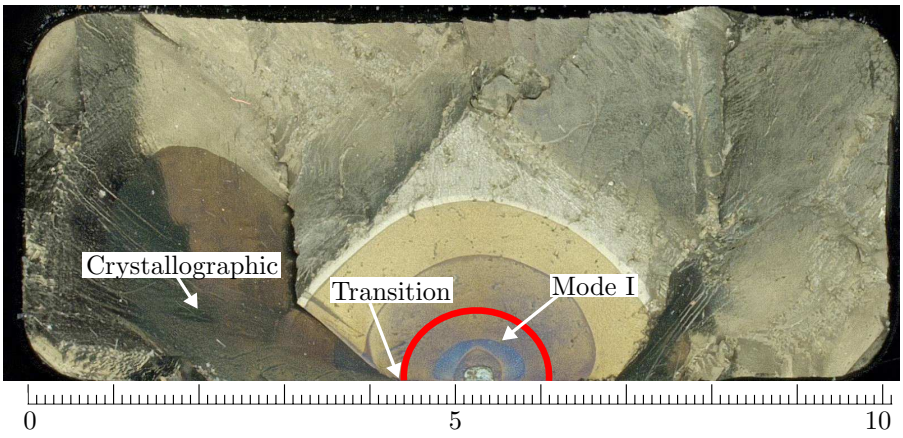

Figure 5: Illustration of the approximated crack front shape (marked in red) at cracking mode transition in Kb3-6. Unit of the scale in mm.

by Reed *et. al* [18], and is motivated by the assumption that shearing as well as opening contribute to crystallographic cracking, and thus k_{EQ} is to be the decisive measure. Further, they argue that even though k_{EQ} on a given slip system might be very high the corresponding k_{RSS} might be low, *cf.* Eq. 3. Thus, another criterion must be fulfilled to make sure that the shear stresses are sufficiently high, namely that the ratio of k_{RSS} to k_{RNS} must be at least $\sim$0.45.

4. Evaluations and discussion

In order to evaluate the anisotropic SIFs, 3D FE-simulations of the Kb and DCT specimens have been conducted where the boundary conditions have been chosen to represent the experimental setup. Further details about the models can be found in [19]. The anisotropic SIFs were calculated by the crack evaluation tool FRANC3D V7.4 [29] using the FE-solver of ABAQUS V6.12 [30]. All simulations were performed in a linear elastic context using the elastic constants and misalignments given in Table 3 and 1, respectively. The RSIFs k_I, k_{II} and k_{III} were evaluated for each node along the discretized transition crack fronts that were present at cracking mode transition. An example can be seen in Fig. 5,

where the approximated crack geometry is highlighted in red for Kb3-6. Generally, the cracks were approximated to be semi-circular for Kb and as a part of a shallow ellipse for the DCT specimens. Heat tints were applied in some of the experiments, which were utilized as a guidance for the approximation of the crack front shape in the specimens.

4.1. k_{RSS} threshold criterion

The RSSIF k_{RSS} was evaluated along the entire crack front at transition for all specimens, and the results can be seen in Fig. 6 as a function of the normalized distance along the crack front, *cf.* Fig. 7. The k_{RSS} values were evaluated corresponding to the three slip systems of the experimentally observed active crystallographic planes, where the maximum of the three k_{RSS} values was used in the evaluations. Note that all 12 slip systems on the four potential crystallographic planes have been evaluated but the focus in this work was on the crystallographic plane observed by the experiments.

It can be seen that the k_{RSS} values for the transition crack lengths are lower for the Kb specimens compared to the DCT specimens. One exception is DCT30 that gives similar results as the Kb specimens. As will be discussed below, this specimen seemed to be an outlier and was disregarded in the following. In general, the k_{RSS} values fluctuate more for the Kb specimens and gives more straight curves for the DCT specimens. This is due to the crack front shape and that the angle it intersects with the crystallographic planes is more or less constant for the DCT specimens and deviating considerably for the Kb specimens with their semi-circular crack fronts. Fig. 6 mainly serves to give the reader an understanding about the through thickness behaviour of the k_{RSS} values.

As crystallographic crack growth usually initiates at the free surfaces [8, 14] emphasis was given towards this area, *i.e.* three evaluation nodes close to the free surfaces, *cf.* Fig. 7, were used to represent the area of the cracking mode transition. The average of the k_{RSS} values obtained from the three evaluation nodes was used to smooth out the results for each specimen. Note that the node at the free surface was omitted since the order of the present singularity changes

and more importantly distorted elements can generate inaccurate values. The evaluation nodes are shown in Fig. 8, where they are highlighted together with the crack front elements and the crack front on the FE-mesh for the transition crack of Kb07. The mean value and Standard Deviation (SD) were determined for each specimen geometry. This means that for the three Kb specimens the averaged (over the evaluation nodes) k_{RSS} values were considered and, based on those, the mean and SD was calculated. The same was done according to the DCT specimens and the combined data of Kb and DCT. This has been done to give the reader a feeling of the scatter present in terms of the SD corresponding to the mean value. The results are shown in Fig. 9a), where the separate experiments are represented by the asterisks, the mean value per specimen group by the squares and the 95% confidence interval (based on the SD) is given by

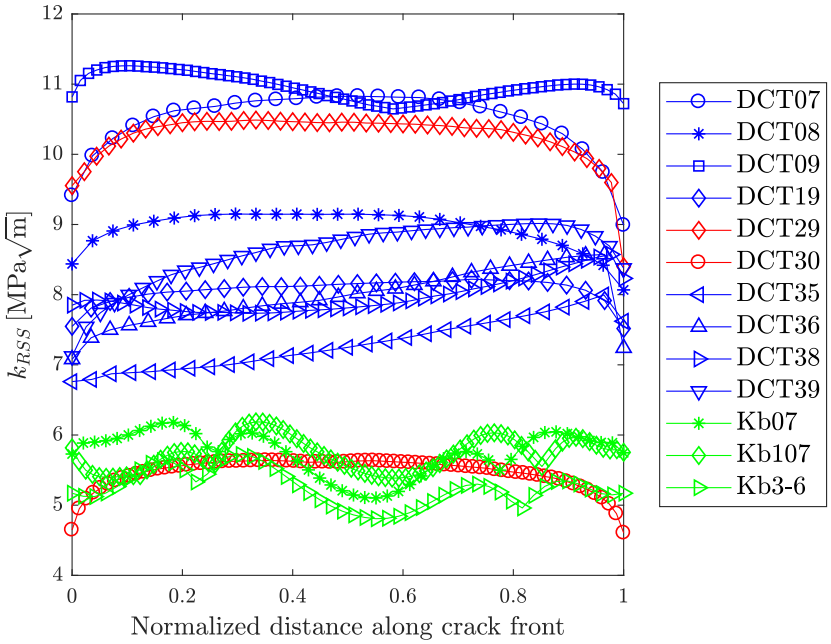

Figure 6: k_{RSS} as a function of of the normalized distance along the transition crack front. See Fig. 7 for the an example of the transition crack length and the definition of the x-axis which ranges from 0 to 1.

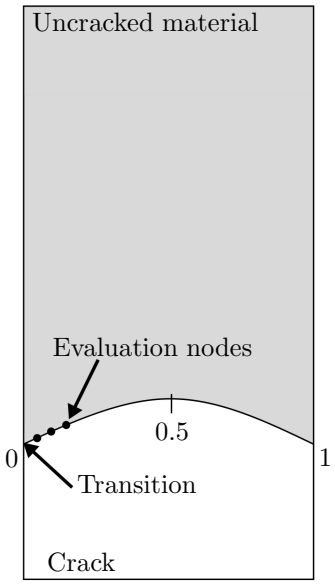

Figure 7: Illustration of the normalized distance along the crack front and the evaluation nodes at the cracking mode transition for a cracked DCT specimen.

the interval indicators. For Kb, DCT and the combined data (Kb and DCT) the values were calculated to 5.5 ± 0.4 (mean $\pm$ SD), 8.7 ± 1.4 and 7.9 ± 1.9, respectively, with the unit MPa$\sqrt{\text{m}}$. Considering the data points for the DCT specimens, it can be seen that the above mentioned DCT30 (marked by the red ring) lies far off and is thus disregarded as an outlier. The nature of this is unclear, but might be related to the testing where it was difficult to initiate the crack growth. It is assumed, that an overload at room temperature occurred during the precracking that could have influence the transition behaviour. Further, it can be seen that the k_{RSS} values at transition collapse with a small SD for the Kb specimen and higher scatter is present for the DCT specimens. However, it should be noted that there are fewer data points for the Kb compared to the DCT specimens.

Following the argument by Telesman and Ghosn [9] as discussed above, the RSSIFs were also sorted by loading frequencies in Fig. 9b) in decreasing order. The mean and 95% confidence interval were evaluated to be 5.52 ± 0.38 (mean

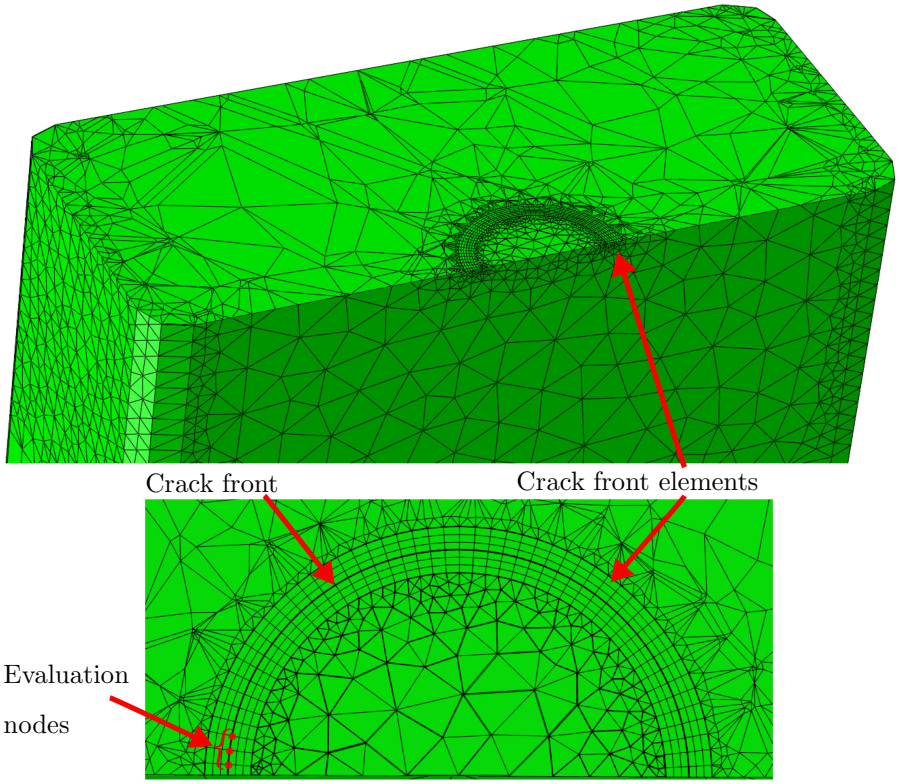

Figure 8: Crack front mesh with highlighted evaluation nodes for the transition crack front of Kb07.

$\pm$ SD), 7.7 ± 0.7 and 9.5 ± 1.3 for $f = 0.5$ Hz, $f = 0.1$ Hz and $f = 0.025$ Hz respectively, with the unit MPa$\sqrt{\text{m}}$. The tendency as described by Telesman and Ghosn can be observed, where a higher frequency favours crystallographic crack growth, *i.e.* transition at lower k_{RSS} values. The authors are aware of the small sample size and are thus not concluding a frequency dependency, but rather pointing out the observed trend that is present in the results. This needs to be studied in more detail based on more experiments and loading frequencies. Despite the trend, it should also be noted that the difference in loading frequency is not of great magnitude.

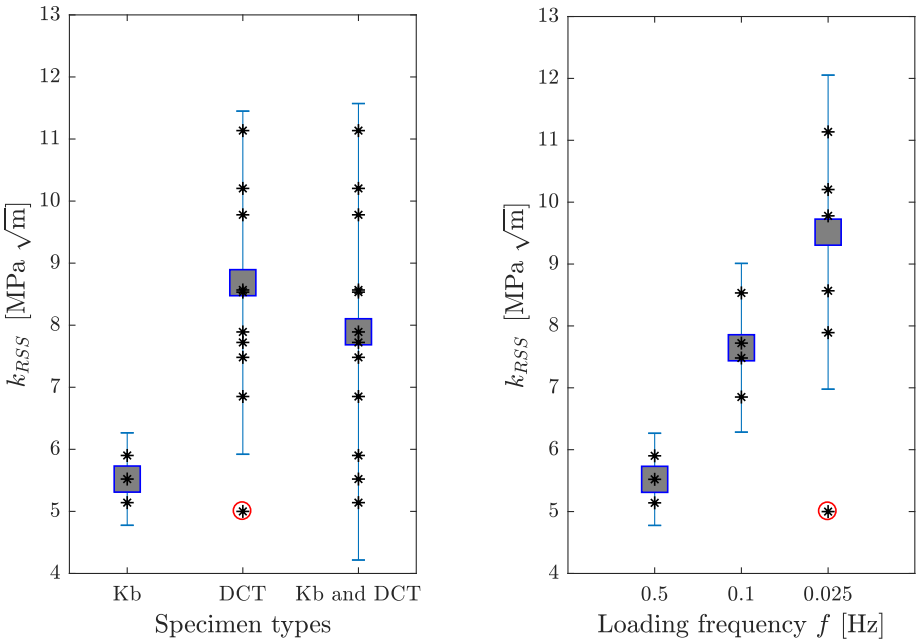

(a) (b)

Figure 9: Representation of the mean and 95% confidence interval of the k_{RSS} values at the cracking mode transition in the vicinity of the free surface with respect to a) specimen types and b) loading frequencies.

Nevertheless, considering all data points a conservative conclusion can be that at the threshold value of $k_{RSS} \approx 4.2$ MPa$\sqrt{\text{m}}$ there is risk for a transition to crystallographic crack growth, corresponding to the lower bound of the 95% confidence interval.

4.2. FCGR criterion

The ratio of the crystallographic FCGR to the Mode I FCGR, *cf.* Eq. 6, was evaluated in the same fashion as presented for the k_{RSS} threshold criterion, *i.e.* the values of k_{RSS} and K_I were extracted from the evaluation nodes and the average was taken for each specimen. The data points were then plotted with their mean and 95% confidence interval ordered according to specimen types in Fig. 10. A similar trend as in the k_{RSS} threshold criterion evaluation can be observed. This is due to the fact that the k_{RSS} values were the same in both cases but scaled by C_c and n_c for the crystallographic FCGR. Further, the ratio of k_{RSS} to K_I is similar for all specimens with a corresponding crystallographic orientation. It should be noted that a skewed normal distribution is present as many values are close to zero. This leads to a situation where the 95% confidence interval includes negative values when considering all data points (Kb and DCT), *cf.* Fig. 10a). Nevertheless, the same procedure was chosen to present the data as it enables a comparison to the k_{RSS} threshold criterion. For Kb, DCT and the combined data (Kb and DCT) the values were calculated to 1.6 ± 0.4 (mean $\pm$ SD), 5.7 ± 2.6 and 4.7 ± 2.9, respectively. Compared to the k_{RSS} threshold criterion the SDs are comparable for the Kb specimen but higher for the DCT specimens and the combined data. The mean value for the combined data is 4.7 which means that a transition of cracking modes occurs once the crystallographic FCGR is 4.7 times the one of Mode I. As for the k_{RSS} threshold criterion the evaluations of the rate ratio X were plotted versus the loading frequencies in Fig. 10b) in decreasing order. The mean and 95% confidence interval were evaluated to be 1.6 ± 0.4 (mean $\pm$ SD), 3.8 ± 1.5 and 7.2 ± 2.4 for $f = 0.5$ Hz, $f = 0.1$ Hz and $f = 0.025$ Hz, respectively. Again, a clear tendency can be observed with favoured crystallographic cracking at lower

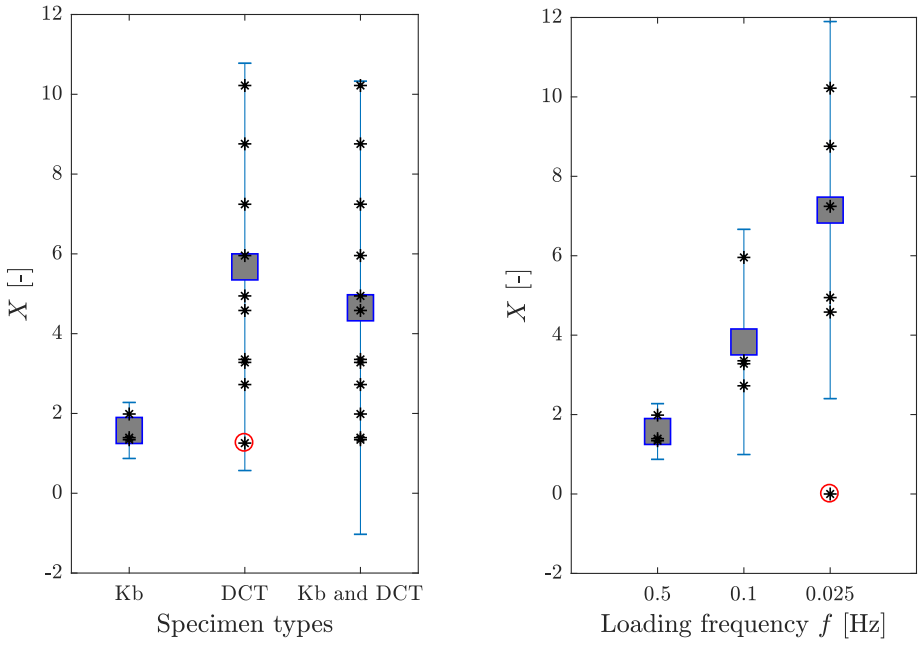

Figure 10: Representation of the mean and 95% confidence interval of the rate ratio X at the cracking mode transition in the vicinity of the free surface with respect to a) specimen types and b) loading frequencies.

values of the rate ratio X for higher frequencies. A drawback with this criterion is the strong dependency on the crystallographic crack growth model, *cf.* Eq. 4, where the parameters C_c and n_c have been evaluated in Busse *et al.* [17] based on experiments on Kb specimens alone.

4.3. Two-factor criterion

This criterion accounts for the RSSes as well as the RNSes by evaluating the ratio k_{RSS}/k_{RNS} as a function of k_{EQ}. The value of k_{EQ} was evaluated along all slip systems on the active crystallographic planes and the maximum value was chosen. The same slip system was then chosen to evaluate the associated values of k_{RSS} and k_{RNS}. The results can be seen in the left plot in Fig. 11. The shaded area indicates a risk for transition of cracking modes and corresponds to

the minimum value of $k_{EQ} \approx 14.3$ MPa$\sqrt{\text{m}}$ and a k_{RSS}/k_{RNS} ratio of at least $\sim$0.11. The mean and SD for k_{EQ} are 23.0 ± 5.7 MPa$\sqrt{\text{m}}$ showing that there is a large scatter.

In much of the available literature it has been found that k_{RSS} is favoured as the deciding measure for crystallographic cracking [17, 31]. Hence, the same investigation was also performed with k_{RSS} instead of k_{EQ}. Here, the slip systems that were evaluated were the ones that yielded the highest k_{RSS} value, thus the ratio of k_{RSS} to k_{RNS} also changes accordingly [19]. In the right plot in Fig. 11 it can be seen that the shaded area indicating risk for crystallographic cracking decreased substantially compared to the analysis associated with k_{EQ}. The mean and SD for k_{RSS} are 7.9 ± 1.9 MPa$\sqrt{\text{m}}$ (mean $\pm$ SD) indicating a decrease in scatter. The same scale on the y-axis has been used in the two

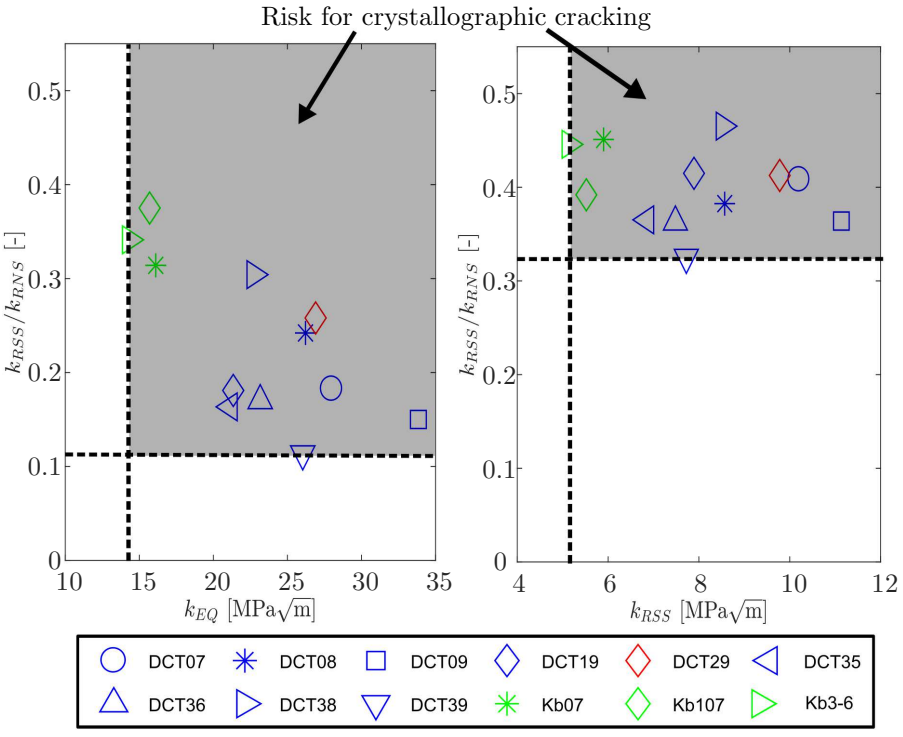

Figure 11: The ratio k_{RSS}/k_{RNS} as a function of k_{EQ} (left) and k_{RSS} (right) for all specimens, where the shaded areas indicates a risk for crystallographic cracking.

Table 4: Comparison of the investigated measures at cracking mode transition for all specimen with respect to their mean, SD and CV.

Criterion	Measure	Mean	SD	CV [-]
k_{RSS} threshold	k_{RSS} [MPa$\sqrt{\text{m}}$]	7.89	1.88	0.24
FCGR	X [-]	4.65	2.89	0.62
Two-factor	k_{EQ} [MPa$\sqrt{\text{m}}$]	23.0	5.7	0.25

graphs in Fig. 11 to enable a better comparison.

4.4. Comparison of the criteria

In order to compare the scatter in the evaluations of the different criteria a statistical measure was introduced that is independent from the unit and accounts for the magnitude of the statistical values. In this work, the Coefficient of Variation (CV) was used and is calculated by the ratio of SD/mean [32]. Comparing all three criteria it can be said that the k_{RSS} threshold model gives the lowest CV and consequently the least scatter when considering all specimens, *cf.* Table 4. Further, this criterion is most applicable as it only depends on one deciding parameter, whereas the two-factor criterion depends on two and the FCGR criterion depends on the associated FCGRs. However, compared to the k_{RSS} threshold criterion, the two-factor criterion can give a more accurate indication for a transition of cracking modes in certain cases. This is due to the second criterion, where the data points that give a k_{RSS} over the threshold but a low k_{RSS} to k_{RNS} ratio are excluded. It can be mentioned that the criteria were evaluated for different crystallographic orientations and still gave reasonable scatter.

In the FCGR and the k_{RSS} threshold criterion a clear tendency towards a frequency dependency of the cracking mode transition could be observed. The small sample size of only three different frequencies does however not allow for a conclusive argument to be made. Also, as mentioned above, the frequencies did not differ to a great extent which makes the results further inconclusive. Nonetheless, a tendency was observed, which needs to be further evaluated

with more experiments using different loading frequencies to determine if it is significant.

4.5. Final remarks

As can be seen in the presented results there is a large scatter for the DCT specimens compared to the Kb specimens, and also a deviation between these specimen types. This can have several reasons; the Kb specimens are from a different material batch and were also tested in a different facility. Further, the difference in specimen geometry is assumed to impact the results as different constraints are present. Also, the DCT specimens are thin and the crack is taking a larger percentage of the cross-section area with the through cracks compared to the semi-circular cracks in the Kb specimens. It has also been observed that in some DCT specimens the Mode I crack deviated considerably from the anticipated Mode I plane perpendicular to the loading direction. This is believed to be partly due to the anisotropic material behaviour but it is also assumed to be caused by the experimental procedure as *e.g.* friction at the loading pins can have an influence. Further, after a formation of a crystallographic crack the compliance of the DCT specimens can change severely where the two opposite crack flanks do not match any longer due to a rotation of the specimen during the testing and surface induced crack closure might become an issue. An example of this is depicted in Fig. 12 for DCT07.

In this testing campaign it has been observed that the DCT testing is more susceptible to problems in the experimental procedure, as *e.g.* a bending or friction in the loading pins can cause scatter. Due to the small size of the specimens, problems when applying the load can have a high impact on the experimental results. As mentioned above, an overload was assumed to have caused the deviating results in DCT30. Another source of scatter can be the evaluation of the crystallographic orientation which has been performed by measuring the visible dendrites on three orthogonal specimen surfaces, see [19]. As there can be low-angle grain boundaries due to inhomogeneous solidification during the casting procedure present, the local crystallographic orientation at the crack front can

deviate from the one evaluated at the surfaces. It should be mentioned, that $k = k_{max}$ was used in this study for the two-factor and k_{RSS} threshold criterion, and not $\Delta k = k_{max} - k_{min}$ as only low loading ratios $R_\sigma = 0.05$ and 0.1 were considered, *cf.* Table 2. Some of the research also favours plane stress RSIF [8, 18] as the transition originates from the specimen surfaces. However, plane stress conditions only exist at a singular point at the free surface where it is difficult to generate well-shaped elements and extract an accurate material response. Thus, plane strain is assumed to hold true all the way to the free surface as the node at the free surface was excluded from the evaluations as discussed above. Finally, it should be mentioned that, in contrast to the finding by Palmert *et al.* [15] as described above, most other research concluded that the propensity for crystallographic crack growth increases even further as the temperature decreases below 500°C. The nature of the deviating trend is still a topic of future research but might be attributed to the specific alloy studied in this work as well as in [15] and its properties.

Figure 12: Side view of the crack in DCT07 where it can be seen that the two opposite crack flanks do not match due to a rotation of the specimen during testing. This is highlighted by white markers indicating corresponding points on the crack flanks.

5. Conclusions

Three criteria to indicate a transition from Mode I to crystallographic cracking have been evaluated and compared. The main outcomes of this study are:

1. The use of k_{RSS} as a threshold for the transition of cracking modes gives the lowest scatter for all evaluated criteria.
2. The FCGR criterion is least robust as it depends on the previous evaluations of the FCGR of both fracture modes.
3. The Two-Factor criterion yielded less scatter with k_{RSS} compared to k_{EQ} as the deciding measure. Compared to the k_{RSS} threshold model it is more difficult to evaluate, but can be more accurate in certain cases.
4. A tendency towards a loading frequency dependency of the transition could be observed but due to the low sample size no conclusive argument could be made. Further research including more experiments using different loading frequencies is needed.
5. More experimental data is needed to develop a robust criterion that can indicate the risk for a transition of cracking modes with a higher accuracy.

Acknowledgements

This research has been funded by Linköping University and Siemens Industrial Turbomachinery AB, the support of which is gratefully acknowledged. The authors would also like to thank Dr. Paul Wawrzynek at Fracture Analysis Consultants Inc. for all his support and Rodger Romero Ramirez for his help with the laboratory work.

References

[1] A. Pineau, S. D. Antolovich, High temperature fatigue of nickel-base superalloys - A review with special emphasis on deformation modes and oxidation, Engineering Failure Analysis 16 (2009) 2668–2697.

[2] D. Leidermark, J. Moverare, K. Simonsson, S. Sjöström, S. Johansson, Room temperature yield behaviour of a single-crystal nickel-base superalloy with tension/compression asymmetry, Computational Materials Science 47 (2009) 366–372.

[3] D. P. Pope, S. S. Ezz, Mechanical properties of Ni3Al and nickel-base alloys with high volume fraction of gamma prime, International metals reviews 29 (1984) 136–167.

[4] M. Segersäll, J. Moverare, D. Leidermark, K. Simonsson, Low-cycle fatigue behaviour of a Ni-based single-crystal superalloy, Advanced Materials Research 891-892 (2014).

[5] D. Leidermark, M. Segersäll, Modelling of thermomechanical fatigue stress relaxation in a single-crystal nickel-base superalloy, Computational Materials Science 90 (2014) 61–70.

[6] R. L. Amaro, S. D. Antolovich, R. W. Neu, A. Staroselsky, Physics-Based Modeling of Thermo-Mechanical Fatigue in PWA 1484, in: Superalloys 2012, 2012, pp. 481–490. doi:10.1002/9781118516430.ch53.

[7] B. F. Antolovich, A. Saxena, S. D. Antolovich, Fatigue crack propagation in single-crystal CMSX- 2 at elevated temperature, Journal of Materials Engineering and Performance 2 (1993) 489–495.

[8] J. Telesman, L. J. Ghosn, The unusual near-threshold FCG behavior of a single crystal superalloy and the resolved shear stress as the crack driving force, Engineering Fracture Mechanics 34 (1989) 1183–1196.

[9] J. Telesman, L. J. Ghosn, Fatigue crack growth behavior of PWA 1484 single crystal superalloy at elevated temperatures, Journal of Engineering for Gas Turbines and Power 118 (1996) 399–405.

[10] D. Leidermark, J. Moverare, K. Simonsson, S. Sjöström, A combined critical plane and critical distance approach for predicting fatigue crack initia-

tion in notched single-crystal superalloy components, International Journal of Fatigue 33 (2011) 1351–1359.

[11] T. Tinga, Stress intensity factors and crack propagation in a single crystal nickel-based superalloy, Engineering Fracture Mechanics 73 (2006) 1679–1692.

[12] H. Kagawa, Y. Mukai, The Effect of Crystal Orientation and Temperature on Fatigue Crack Growth of Ni-Based Single Crystal Superalloy, in: Superalloys 2012, John Wiley and Sons, 2012, pp. 225–233. doi:10.1002/9781118516430.ch25.

[13] K. S. Chan, J. Feiger, Y. D. Lee, R. John, S. J. Hudak, Fatigue crack growth thresholds of deflected mixed-mode cracks in PWA1484 127 (2005) 2–7.

[14] R. W. Neu, Crack paths in single-crystal Ni-base superalloys under isothermal and thermomechanical fatigue, International Journal of Fatigue 123 (2019) 268–278.

[15] F. Palmert, J. Moverare, D. Gustafsson, C. Busse, Fatigue crack growth behaviour of an alternative single crystal nickel base superalloy, International Journal of Fatigue 109 (2018) 166–181.

[16] D. MacLachlan, D. Knowles, Fatigue behaviour and lifing of two single crystal superalloys, Fatigue and Fracture of Engineering Materials and Structures 24 (2001).

[17] C. Busse, F. Palmert, B. Sjödin, P. Almroth, D. Gustafsson, K. Simonsson, D. Leidermark, Evaluation of the crystallographic fatigue crack growth rate in a single-crystal nickel-base superalloy, International Journal of Fatigue 127 (2019) 259–267.

[18] P. A. Reed, X. D. Wu, I. Sinclair, Fatigue crack path prediction in UDIMET 720 nickel-based alloy single crystals, Metallurgical and Materials Transactions A: Physical Metallurgy and Materials Science (2000).

[19] C. Busse, F. Palmert, B. Sjödin, P. Almroth, D. Gustafsson, K. Simonsson, D. Leidermark, Prediction of crystallographic cracking planes in single-crystal nickel-base superalloys, Engineering Fracture Mechanics 196 (2018) 206–223.

[20] Q. Chen, H. Liu, Resolved shear stress intensity coefficient and fatigue crack growth in large crystals, Theoretical and Applied Fracture Mechanics 10 (1988) 111–122.

[21] X. Chen, M. Sakaguchi, Transition behavior from Mode I cracking to crystallographic cracking in a Ni-base single crystal superalloy, International Journal of Fatigue 132 (2020) 105400.

[22] C. Busse, J. Homs, D. Gustafsson, F. Palmert, B. Sjödin, J. Moverare, K. Simonsson, D. Leidermark, A finite element study of the effect of crystal orientation and misalignment on the crack driving force in a single-crystal superalloy, in: Proceedings of the ASME Turbo Expo, volume 7A-2016, 2016. doi:10.1115/GT2016-56305.

[23] S. Suzuki, M. Sakaguchi, H. Inoue, Temperature dependent fatigue crack propagation in a single crystal Ni-base superalloy affected by primary and secondary orientations, Materials Science and Engineering A (2018).

[24] R. Reed, J. Moverare, A. Sato, F. Karlsson, M. Hasselqvist, A New Single Crystal Superalloy for Power Generation Applications, in: Superalloys 2012, 2012, pp. 197–204.

[25] A. Coles, R. E. Johnson, H. G. Popp, Utility of surface-flawed tensile bars in cyclic life studies, Journal of Engineering Materials and Technology, Transactions of the ASME 98 (1976) 305–315.

[26] ASTM E647-13, Standard Test Method for Measurement of Fatigue Crack Growth Rates, American Society for Testing and Materials (2014).

[27] L. Banks-Sills, P. A. Wawrzynek, B. Carter, A. R. Ingraffea, I. Hershkovitz, Methods for calculating stress intensity factors in anisotropic materials:

Part II-Arbitrary geometry, Engineering Fracture Mechanics 74 (2007) 1293–1307.

[28] A. Hoenig, Near-tip behavior of a crack in a plane anisotropic elastic body, Engineering Fracture Mechanics 16 (1982) 393–403.

[29] FRANC3D, FRANC3D Reference Manual, Fracture Analysis Consultants Inc., Ithaca, USA, 2016.

[30] ABAQUS, ABAQUS 6.12 Documentation, Dassault Systèmes, Providence, USA, 2014.

[31] M. Sakaguchi, R. Komamura, X. Chen, M. Higaki, H. Inoue, Crystal plasticity assessment of crystallographic Stage I crack propagation in a Ni-based single crystal superalloy, International Journal of Fatigue (2019).

[32] B. Everitt, The Cambridge Dictionary of Statistics, Cambridge University Press, Cambridge, U.K. ; New York, 1998.